J|A|C|S
ARTICLES
Published on Web 01/24/2006

Resonating Valence Bond Ground State in Oxygen-Functionalized Phenalenyl-Based Neutral Radical Molecular Conductors

Swadhin K. Mandal,[†] Satyabrata Samanta,[†] Mikhail E. Itkis,[†] Dell W. Jensen,[‡] Robert W. Reed,[§] Richard T. Oakley,[§] Fook S. Tham,[†] Bruno Donnadieu,[†] and Robert C. Haddon*,[†]

Contribution from the Departments of Chemistry, Chemical & Environmental Engineering, University of California, Riverside, California 92521-0403, Department of Chemistry, University of Kentucky, Lexington, Kentucky 40506-0055, and Department of Chemistry, University of Waterloo, Waterloo, Ontario N2L3G1, Canada

Received September 1, 2005; E-mail: robert.haddon@ucr.edu

Abstract: We report the preparation, crystallization, and solid-state characterization of the first two members of a new family of spiro-bis(1,9-disubstituted phenalenyl)boron neutral radicals based solely on oxygen functionalization, and we show that this strategy significantly lowers the electrochemical disproportionation potentials (ΔE), in comparison with other spiro-bis(1,9-disubstituted phenalenyl)boron salts. In the solid state, these radicals pack in a continuous array of $\pi-\pi$-stacked phenalenyl units with very short intermolecular carbon···carbon contacts. These two radicals are among the most highly conducting neutral organic solids, with room temperature conductivities reaching 0.3 S/cm. Magnetic susceptibility measurements show that the radicals do not exist as isolated free radicals, and there is significant spin−spin interaction between the molecules in the solid state as expected from the crystal structures and the calculated band structures; the solid-state properties are best rationalized in terms of the resonating valence bond model.

Introduction

Most closed shell π-conjugated organic molecules do not form conducting solids owing to their wide HOMO−LUMO gap. Open-shell organic molecules are rare in the solid state, but even in this case, it is unusual to obtain conducting solids because of the strength of the on-site Coulomb repulsion which leads to a Mott insulating ground state; thus most organic molecular conductors are based on charge-transfer salts which require electron transfer between two components (donor and acceptor) to generate charge carriers. In fact, both components can be incorporated into a single molecule which undergoes internal charge transfer, as in the case of single component conductors based on dithiolate ligands.[1−5]

Single component molecular conductors based on neutral radical building blocks represent an appealing alternative to conventional charge-transfer organic conductors and superconductors, in which the unpaired electrons of the neutral radicals serve as charge carriers.[6,7] Sulfur−nitrogen radicals were the first class of compounds to show conductivity based on this principle.[8] The idea of using the phenalenyl system as a building block for designing intrinsic molecular conductors and superconductors is not only appealing but also challenging,[6,7] and this system has attracted theoretical and experimental attention.[9−14]

Phenalenyl is a well-known odd alternant hydrocarbon with high symmetry (D_{3h}) which has the ability to form three redox species: cation, radical, and anion.[15−17] Such characteristic

[†] University of California, Riverside.
[‡] University of Kentucky.
[§] University of Waterloo.

(1) Tanaka, H.; Okano, Y.; Kobayashi, H.; Suzuki, W.; Kobayashi, A. *Science* **2001**, *291*, 285−287.
(2) Tanaka, H.; Tokumoto, M.; Ishibashi, S.; Graf, D.; Choi, E. S.; Brooks, J. S.; Yasuzuka, S.; Okano, Y.; Kobayashi, H.; Kobayashi, A. *J. Am. Chem. Soc.* **2004**, *126*, 10518−10519.
(3) Kobayashi, A.; Sasa, M.; Suzuki, W.; Fujiwara, E.; Tanaka, H.; Tokumoto, M.; Okano, Y.; Fujiwara, H.; Kobayashi, H. *J. Am. Chem. Soc.* **2004**, *126*, 426−427.
(4) Llusar, R.; Uriel, S.; Vicent, C.; Clemente-Juan, J. M.; Coronado, E.; Gòmez-García, C. J.; Braïda, B.; Canadell, E. *J. Am. Chem. Soc.* **2004**, *126*, 12076−12083.
(5) Kobayashi, A.; Fujiwara, E.; Kobayashi, H. *Chem. Rev.* **2004**, *104*, 5243−5264.
(6) Haddon, R. C. *Nature* **1975**, *256*, 394−396.
(7) Haddon, R. C. *Aust. J. Chem* **1975**, *28*, 2343−2351.
(8) Oakley, R. T. *Can. J. Chem.* **1993**, *71*, 1775−1784.
(9) Goto, K.; Kubo, T.; Yamamoto, K.; Nakasuji, K.; Sato, K.; Shiomi, D.; Takui, T.; Kubota, M.; Kobayashi, T.; Yakusi, K.; Ouyang, J. *J. Am. Chem. Soc.* **1999**, *121*, 1619−1620.
(10) Morita, Y.; Aoki, T.; Fukui, K.; Nakazawa, S.; Tamaki, K.; Suzuki, S.; Fuyuhiro, A.; Yamamoto, K.; Sato, K.; Shiomi, D.; Naito, A.; Takui, T.; Nakasuji, K. *Angew. Chem., Int. Ed.* **2002**, *41*, 1793−1796.
(11) Fukui, K.; Sato, K.; Shiomi, D.; Takui, T.; Itoh, K.; Gotoh, K.; Kubo, T.; Yamamoto, K.; Nakasuji, K.; Naito, A. *Synth. Met.* **1999**, *103*, 2257−2258.
(12) Koutentis, P. A.; Chen, Y.; Cao, Y.; Best, T. P.; Itkis, M. E.; Beer, L.; Oakley, R. T.; Brock, C. P.; Haddon, R. C. *J. Am. Chem. Soc.* **2001**, *123*, 3864−3871.
(13) Takano, Y.; Taniguchi, T.; Isobe, H.; Kubo, T.; Morita, Y.; Yamamoto, K.; Nakasuji, K.; Takui, T.; Yamaguchi, K. *J. Am. Chem. Soc.* **2002**, *124*, 11122−11130.
(14) Takano, Y.; Taniguchi, T.; Isobe, H.; Kubo, T.; Morita, Y.; Yamamoto, K.; Nakasuji, K.; Takui, T.; Yamaguchi, K. *Chem. Phys. Lett.* **2002**, *358*, 17−23.
(15) Reid, D. H. *Quart. Rev.* **1965**, *19*, 274−302.
(16) Reid, D. H. *Chem. Ind.* **1956**, 1504−1505.
(17) Reid, D. H. *Tetrahedron* **1958**, *3*, 339−352.

10.1021/ja0560276 CCC: $33.50

Scheme 1

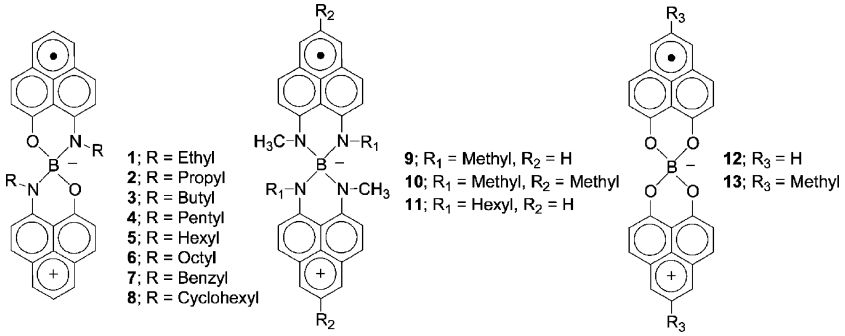

features have been widely utilized for exploring new conjugated electronic systems, such as multifunctional electronic and magnetic materials.[18] Certain paramagnetic phenalenyl radicals undergo facile dimerization either by π-association or by σ-association. Recent progress in phenalenyl chemistry[9−14,19] has led to the isolation of the radical itself in the crystalline state through the introduction of bulky substituents.[9,10,12] In fact, the intermolecular π-association of 2,5,8-tri-*tert*-butylphenalenyl radicals can take place either by formation of a two-electron bond to form a π-dimer (radical−radical pair) or by formation of a one-electron bond to form a π-pimer (radical−cation pair).[19]

In the pursuit of our goal of realizing phenalenyl-based neutral radical intrinsic molecular conductors, we have reported two different families of spiro-bis(1,9-disubstituted phenalenyl)boron neutral radicals (**1**−**11**, Scheme 1).[20−27] The spiro-conjugation at the boron center leads to an intramolecular $\pi-\pi$ energy level splitting of ∼0.5 eV,[28] and the lower level becomes the singly occupied molecular orbital (SOMO). Unlike conventional neutral radicals, in the solid state the spiro-conjugated biphenalenyls give rise to a quarter-filled energy band, and this significantly reduces the on-site Coulomb correlation energy (U), which is usually responsible for the insulating ground state that occurs in half-filled band structures. The spiro-geometry severely inhibits the one-dimensional packing (see **7**)[24] that is characteristic of many organic charge-transfer salts.

Since the discovery of the first boron-containing neutral radical molecular conductor (**5**),[20] we have reported a class of π-dimeric neutral radical molecular conductors (**1** and **3**) differing only in the length of the alkyl groups (Scheme 1).[21] These π-dimeric neutral radicals (**1** and **3**) simultaneously exhibit bistability in three physical channels: magnetic, electrical, and optical,[18] which has been rarely realized in a single system.[29] The bistability in these crystals (**1** and **3**) originates from a phase transition between high-temperature paramagnetic states and low-temperature diamagnetic states, with an increase of conductivity at the phase transition. Recently, we reported the first example of light-mediated crystallization, which is dependent on C−C σ-bond formation between radicals (**6**).[25] Thus **6** exists as two different forms, namely, a free radical semiconductor and a σ-dimerized insulator, and their formation is dictated by the absence or presence of light at the instant of crystallization. The preparation, crystallization, and solid-state characterization of the first members of a new family of spiro-bis(1,9-diamino-substituted-phenalenyl)boron neutral radicals (**9**−**11**) have been reported.[26] The measured conductivities of these neutral radicals (**9**−**11**) correlate with the closest intermolecular contacts in the solid state and with the calculated band dispersions, even though the bandwidths are much smaller than those found in typical organic conductors (as in **1**−**6**).

The distinctive features of the molecular solids **1**−**6** and **9**−**11** include the following: (1) the absence of any obvious conducting pathway(s); these radicals do not stack infinitely in the solid state within van der Waals atomic separations, and thus the mechanism of conductivity remains to be explained in this class of compounds; (2) magnetic susceptibility measurements show that these compounds behave as free radicals with one spin per molecule, indicating that there is little spin−spin interaction between the molecules in the solid state; (3) the versatility shown by their lattice arrangement in the solid state and the sensitivity of solid-state packing and properties to small change in the ligand system; for example, the *N*-hexyl-substituted radical **5** shows a conductivity of $\sigma_{RT} = 5 \times 10^{-2}$ S/cm, while radical **4** with a pentyl substituent on nitrogen, just one carbon less in the aliphatic chain, shows a conductivity ($\sigma_{RT} = 4 \times 10^{-7}$ S/cm) which is 5 orders smaller in magnitude than that of **5**; and (4) the difficulty in rationalizing the structures, band structures, magnetism, and conductivity to provide a consistent picture of the electronic structure.

While the compounds discussed above (**1**−**6**, **9**−**11**) fall in the extreme narrow bandwidth limit ($W < 0.1$ eV),[30,31] we have very recently discovered two compounds (**7** and **8**) which show bandwidths which are reminiscent of standard organic conductors and superconductors ($W \sim 0.5$ eV), and below we discuss

(18) Itkis, M. E.; Chi, X.; Cordes, A. W.; Haddon, R. C. *Science* **2002**, *296*, 1443−1445.
(19) Small, D.; Zaitsev, V.; Jung, Y.; Rosokha, S. V.; Head-Gordon, M.; Kochi, J. K. *J. Am. Chem. Soc.* **2004**, *126*, 13850−13858.
(20) Chi, X.; Itkis, M. E.; Patrick, B. O.; Barclay, T. M.; Reed, R. W.; Oakley, R. T.; Cordes, A. W.; Haddon, R. C. *J. Am. Chem. Soc.* **1999**, *121*, 10395−10402.
(21) Chi, X.; Itkis, M. E.; Kirschbaum, K.; Pinkerton, A. A.; Oakley, R. T.; Cordes, A. W.; Haddon, R. C. *J. Am. Chem. Soc.* **2001**, *123*, 4041−4048.
(22) Chi, X.; Itkis, M. E.; Reed, R. W.; Oakley, R. T.; Cordes, A. W.; Haddon, R. C. *J. Phys. Chem. B* **2002**, *106*, 8278−8287.
(23) Chi, X.; Itkis, M. E.; Tham, F. S.; Oakley, R. T.; Cordes, A. W.; Haddon, R. C. *Int. J. Quantum Chem.* **2003**, *95*, 853−865.
(24) Pal, S. K.; Itkis, M. E.; Reed, R. W.; Oakley, R. T.; Cordes, A. W.; Tham, F. S.; Siegrist, T.; Haddon, R. C. *J. Am. Chem. Soc.* **2004**, *126*, 1478−1484.
(25) Liao, P.; Itkis, M. E.; Oakley, R. T.; Tham, F. S.; Haddon, R. C. *J. Am. Chem. Soc.* **2004**, *126*, 14297−14302.
(26) Mandal, S. K.; Itkis, M. E.; Chi, X.; Samanta, S.; Lidsky, D.; Reed, R. W.; Oakley, R. T.; Tham, F. S.; Haddon, R. C. *J. Am. Chem. Soc.* **2005**, *127*, 8185−8196.
(27) Pal, S. K.; Itkis, M. E.; Tham, F. S.; Reed, R. W.; Oakley, R. T.; Haddon, R. C. *Science* **2005**, *309*, 281−284.
(28) Huang, J.; Kertesz, M. *J. Am. Chem. Soc.* **2003**, *125*, 13334−13335.
(29) Miller, J. S. *Angew. Chem., Int. Ed.* **2003**, *42*, 27−29.
(30) Haddon, R. C.; Ramirez, A. P.; Glarum, S. H. *Adv. Mater.* **1994**, *6*, 316−322.
(31) Haddon, R. C.; Siegrist, T.; Fleming, R. M.; Bridenbaugh, P. M.; Laudise, R. A. *J. Mater. Chem* **1995**, *5*, 1719−1724.

in detail their relationship with the compounds reported in the present paper (**12** and **13**).

Recently we reported **7** as the first one-dimensional phenalenyl-based neutral radical molecular conductor;[24] in the solid state, phenalenyl units of **7** pack parallel to one another in the *y*-direction in a π-step stack structure with inefficient π-overlap. More recently, we reported the cyclohexyl-substituted radical **8**, revealing a symmetrical crystal structure with a continuous array of $\pi-\pi$-stacked superimposed phenalenyl units and short intermolecular carbon···carbon contacts (~3.28 Å).[27] Compound **8** displays temperature-independent Pauli paramagnetism characteristic of a metal. Extended Hückel calculation indicated that compound **8** is a three-dimensional organic metal with a bandwidth of ~0.5 eV. Nevertheless, **8** showed semiconducting behavior with activation energy of 0.054 eV and measured optical energy gap of 0.34 eV. These apparently contradictory properties were best resolved in terms of the resonating valence bond (RVB) ground state postulated by Pauling[32] and Anderson.[33]

Improved conductivities usually result from the design of materials with a higher ratio of *W*/*U*, that is, by increasing the bandwidth *W* or by reducing the on-site Coulomb repulsion, *U*. The bandwidth (*W*) depends on the strength of atomic (or molecular) orbital interactions between neighboring lattice sites and hence is determined by the molecular packing in the solid state. In conventional inorganic metals, such as Cu or Na, the atomic orbitals interact with each other to form broad electronic energy bands of width $W > 3$ eV.[34] These materials are good conductors and can be viewed as crystallized atomic free radicals or cations in a sea of labile electrons. On the other hand, for organic solids, such as the charge-transfer salts, the interactions between the molecules are weak, forming narrow bands ($W \sim 0.5$ eV) in comparison with the inorganic metals. The on-site Coulomb repulsion, *U*, can be loosely equated with the electrochemically measurable solution-based disproportionation potential (ΔE), and for purely neutral systems in order to improve conductivities, the need to design systems with lower ΔE is clear.[35−38] We have therefore pursued the development of stable neutral radicals based on a phenalenyl system in which *U* is minimized and *W* is maximized.

In the present paper, we report the synthesis, electrochemistry, crystallization, and solid-state properties of the first two radicals (**12** and **13**) of a new family of spiro-bis(1,9-disubstituted phenalenyl)boron neutral radicals bearing the phenalenyl-based O,O-ligand system (Scheme 1).[39] Interestingly, the observed disproportionation potentials (ΔE) obtained from electrochemistry are significantly lower than those observed for salts of previously reported spiro-bis(1,9-disubstituted phenalenyl)boron neutral radicals (**1**−**11**). In the solid state, these radicals neither remain strictly monomeric nor do they form simple σ- or π-dimers. The X-ray structures show that these radicals pack in a continuous array of $\pi-\pi$-stacked neighboring phenalenyl units with intermolecular carbon···carbon contacts shorter than the sum of the van der Waals atomic separation, thus forming a polymeric network and providing a conduction pathway that includes the spiro-linkage of the phenalenyl units. Magnetic susceptibility measurements show that these radicals do not exist as isolated free radicals with independent spins, but support the idea of strong spin−spin interactions between individual molecules in the solid state as observed in the solid-state X-ray structures. These two radicals are among the most highly conducting neutral organic solids, and we argue that their properties are best explained in terms of the RVB ground state previously identified in **7** and **8**.[27]

Scheme 2

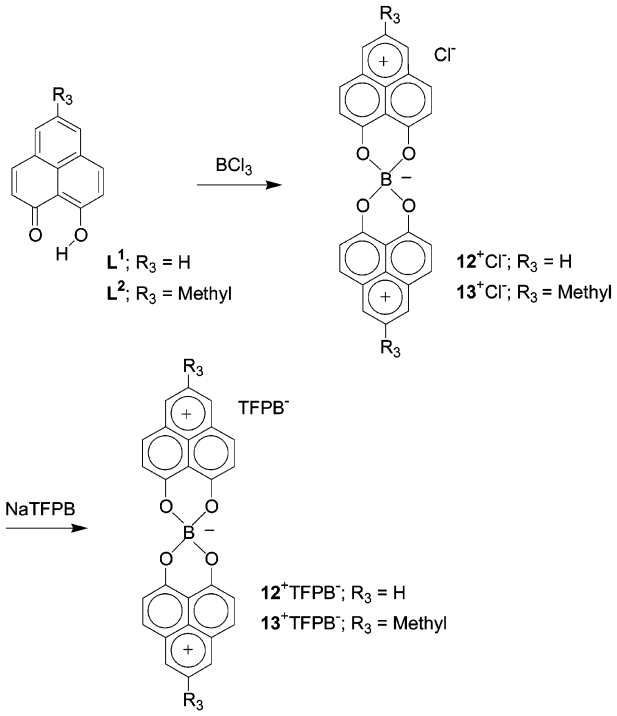

Results and Discussion

Preparation and Electrochemical Properties of Radicals 12 and 13. The syntheses of radicals **12** and **13** followed the same basic principle that has been applied to prepare radicals **1**−**11**.[20,21,24−27] We first prepared the chloride salts (**12**$^+$Cl$^-$ and **13**$^+$Cl$^-$) by following literature methods,[39] and then exchanged the counterion for the tetrakis[3,5-bis(trifluoromethyl)phenyl]-borate (TFPB$^-$) anion to achieve the required solubility properties of the salts (Scheme 2). The TFPB salts (**12**$^+$TFPB$^-$ and **13**$^+$TFPB$^-$) are purified as light-sensitive yellow crystals by recrystallization from ether/hexane mixtures.

The electrochemistry of **12**$^+$TFPB$^-$ and **13**$^+$TFPB$^-$ is presented in Figure 1, where it may be seen that each of these salts shows a well-behaved reversible double reduction corresponding to the successive generation of radical and anion (Scheme 3). The reduction potentials and the disproportionation potentials ($\Delta E^{2-1} = E^2_{1/2} - E^1_{1/2}$) are given in Table 1. As would be expected based on the electronegativities of the substituents, the reduction potentials of the new compounds (**12**$^+$TFPB$^-$ and **13**$^+$TFPB$^-$) occur at less negative potentials than those of **1**$^+$BPh$_4^-$−**11**$^+$BPh$_4^-$, while the disproportionation potentials (ΔE^{2-1}) are lower than those of the previously

(32) Pauling, L. *Nature* **1948**, *161*, 1019−1020.
(33) Anderson, P. W. *Mater. Res. Bull.* **1973**, *8*, 153−160.
(34) Thrower, P. A. *Materials in Today's World*, 2nd ed.; McGraw-Hill's Primis Custom: New York, 1996.
(35) Boere, R. T.; Moock, K. H. *J. Am. Chem. Soc.* **1995**, *117*, 4755−4760.
(36) Chandrasekhar, V.; Chivers, T.; Parvez, M.; Vargas-Baca, I.; Ziegler, T. *Inorg. Chem.* **1997**, *36*, 4772−4777.
(37) Garito, A. F.; Heeger, A. J. *Acc. Chem. Res.* **1974**, *7*, 232−240.
(38) Torrance, J. B. *Acc. Chem. Res.* **1979**, *12*, 79−86.
(39) Haddon, R. C.; Chichester, S. V.; Marshall, J. H. *Tetrahedron* **1986**, *42*, 6293−6300.

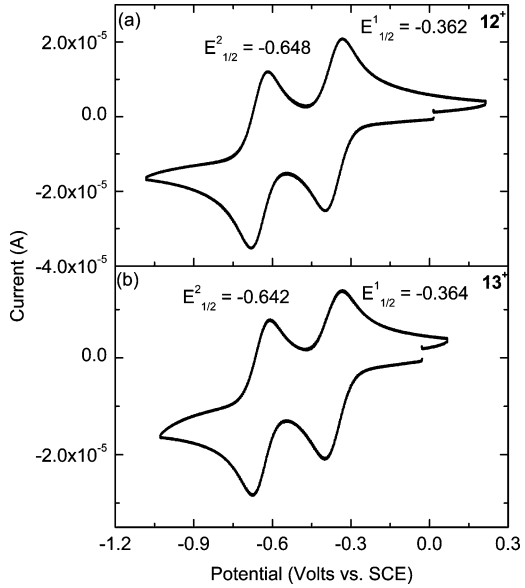

Figure 1. Cyclic voltammetry of (a) **12**$^+$TFPB$^-$ and (b) **13**$^+$TFPB$^-$ in acetonitrile, referenced to SCE via internal ferrocene (not shown).

Scheme 3

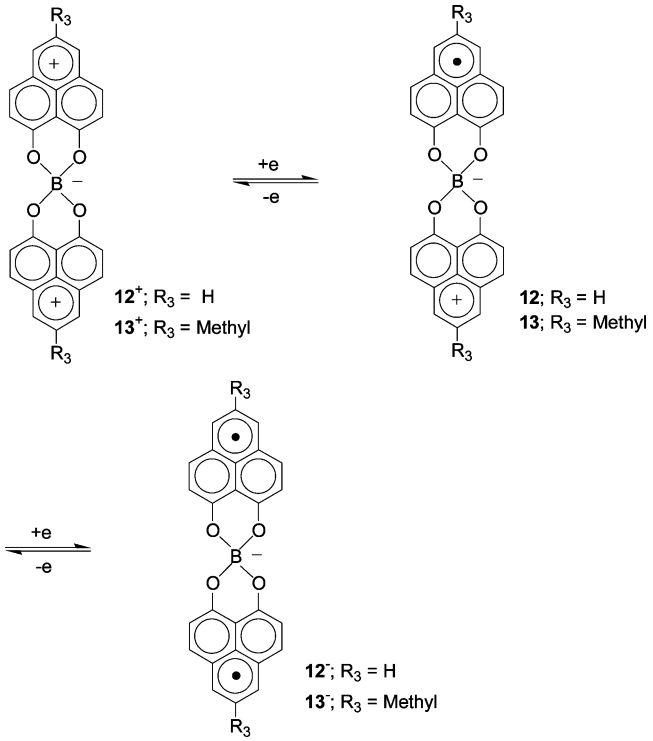

reported salts (**1**$^+$BPh$_4^-$−**11**$^+$BPh$_4^-$). The ΔE^{2-1} value largely determines the on-site Coulombic correlation energy (U) in the solid state, and it is well established as an important discriminator for organic metals.[37,38]

We crystallized the radicals **12** and **13** by reducing the TFPB salts (**12**$^+$TFPB$^-$ and **13**$^+$TFPB$^-$) using the chemical reductant, tetrakis(dimethylamino)ethylene (TDAE),[40] in a H-cell and obtained a moderate yield of high-quality black radical crystals (Scheme 4). To ensure high crystal quality, the H-cell was loaded in a drybox and the solvent (acetonitrile) was degassed

(40) Kolomeitsev, A.; Medebielle, M.; Kirsch, P.; Lork, E.; Roschenthaler, G.-V. *J. Chem. Soc., Perkin Trans. 1* **2000**, 2183−2185.

Table 1. Half-Wave Potentials and Disproportionation Potentials (Volts vs SCE) for Spiro-bis(1,9-disubstituted phenalenyl)boron Salts in CH_3CN

salt	$E^1_{1/2}$	$E^2_{1/2}$	ΔE^{2-1}
1$^+$BPh$_4^-$	−0.75	−1.10	−0.35
2$^+$BPh$_4^-$	−0.75	−1.10	−0.35
3$^+$BPh$_4^-$	−0.73	−1.09	−0.36
5$^+$BPh$_4^-$	−0.74	−1.11	−0.37
6$^+$BPh$_4^-$	−0.74	−1.12	−0.38
7$^+$BPh$_4^-$	−0.68	−1.02	−0.34
8$^+$BPh$_4^-$	−0.75	−1.12	−0.37
9$^+$BPh$_4^-$	−1.02	−1.37	−0.35
10$^+$BPh$_4^-$	−1.06	−1.41	−0.35
11$^+$BPh$_4^-$	−1.01	−1.39	−0.38
12$^+$TFPB$^-$	−0.36	−0.65	−0.29
13$^+$TFPB$^-$	−0.36	−0.64	−0.28

Scheme 4

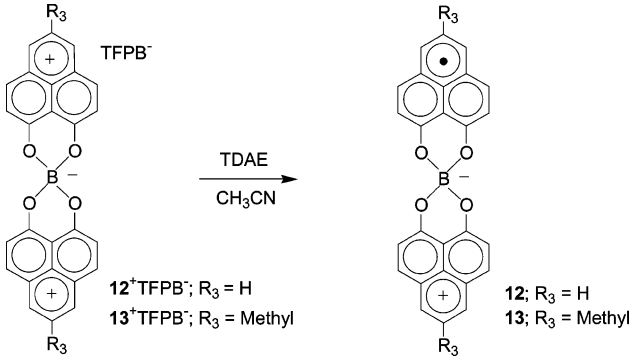

a minimum of three times on a vacuum line before mixing the reductant and salt. Crystal growth started on the glass frit after a few hours, and the crystals reached their optimum size and quality in about 2−3 days. Though solutions of the radical are extremely oxygen sensitive, the crystals are stable enough to allow us to obtain chemical analyses data, X-ray crystal structures, and other solid-state measurements after handling the crystals in the air.

X-ray Crystal Structures of 12 and 13. The structures of **12** and **13** were determined at two different temperatures (100 K and room temperature (RT)) in order to study the interplanar separation as a function of temperature and to test for the presence of phase transitions, such as those observed in the case of **1** and **3**.[21] Table 2 provides crystal data, and Figure 2 shows ORTEP drawings of the radicals **12** and **13**. There are four molecules of **12** and two molecules of **13** in the corresponding unit cells. The most important point for our purposes is the absence of simple σ- or π-dimerization. We did not employ bulky substituents at the active position of the phenalenyl nucleus in order to suppress intermolecular carbon···carbon bond formation.[12,41,42] Carbon-based free radicals usually require steric hindrance to suppress σ-dimerization in the solid state,[9,43] and we are not aware of any other system where resonance stabilization has been sufficient to allow the realization of carbon-based free radicals in the solid state. The asymmetric unit of the molecule **12** is composed of half of the molecule, while the asymmetric unit of molecule **13** consists of the complete molecule, indicating symmetric solid-state packing, particularly in the case of **12**.

(41) Haddon, R. C.; Wudl, F.; Kaplan, M. L.; Marshall, J. H.; Cais, R. E.; Bramwell, F. B. *J. Am. Chem. Soc.* **1978**, *100*, 7629−7633.
(42) Haddon, R. C.; Chichester, S. V.; Stein, S. M.; Marshall, J. H.; Mujsce, A. M. *J. Org. Chem.* **1987**, *52*, 711−712.
(43) Griller, D.; Ingold, K. U. *Acc. Chem. Res.* **1976**, *9*, 13−19.

Table 2. Crystal Data for Radicals **12** and **13**

radical	**12**		**13**	
formula	$C_{26}H_{14}BO_4$		$C_{28}H_{18}BO_4$	
Fw	401.18		429.23	
crystal system	monoclinic		triclinic	
space group	*C*2/*c*		$P\bar{1}$	
Z	4		2	
temp (K)	100(2)	293(2)	100(2)	300(2)
a, Å	16.3665 (13)	16.314(5)	7.3847(3)	7.5018(4)
b, Å	8.7668(7)	8.923(5)	10.7758(5)	10.8505(6)
c, Å	13.0351(9)	13.071(5)	12.6337(6)	12.6187(7)
V, Å^3	1817.4(2)	1849.4(14)	968.96(8)	992.35(9)
α, deg	90.00	90.00	99.3230(10)	95.4420(10)
β, deg	103.655(5)	103.597(5)	99.3230(10)	98.8460(10)
γ, deg	90.00	90.00	99.6940(10)	99.8460(10)
θ range, deg	2.65 to 35.86	2.57 to 28.61	1.65 to 28.28	1.65 to 28.28
indep. reflections	3889	2167	4776	4900
final *R* indices	$R_1 = 0.0494$	$R_1 = 0.0348$	$R_1 = 0.0451$	$R_1 = 0.0444$
[$I > 2\sigma(I)$]	$wR_2 = 0.1289$	$wR_2 = 0.0656$	$wR_2 = 0.1159$	$wR_2 = 0.1051$
R indices	$R_1 = 0.1180$	$R_1 = 0.1915$	$R_1 = 0.0747$	$R_1 = 0.1054$
(all data)	$wR_2 = 0.1575$	$wR_2 = 0.1063$	$wR_2 = 0.1298$	$wR_2 = 0.1263$
mean plane separations, Å	3.17	3.22	3.26, 3.29	3.30, 3.30

The spiro-conjugated phenalenyl rings in molecule **12** are in an almost perpendicular orientation (dihedral angle 89.7°), whereas the rings deviate considerably from the perpendicular orientation (dihedral angle 85.9°) in molecule **13**. The most important difference in the molecular geometries of **12** and **13** arises from the bending of one of the phenalenyl units in **13** at two of its oxygen atoms (O3 and O4, Figure 2b). The angle of bend in **13** is ∼32° (Figure 2b), whereas **12** remains almost planar (the angle of bend at the oxygen atoms is ∼0.9° in **12**). As discussed below, the bending in **13** results from the steric requirements of the 5-methyl substituents.

The solid structure of **12** and **13** reveals that both of these radicals pack in a continuous array of *π*-stacked neighboring phenalenyl units with parallel orientation and very short intermolecular carbon···carbon contacts so as to form a polymeric network of neutral radicals (Figures 3a and 4). It has been previously established that the orientation of the radical molecules in the well-spaced, narrow bandwidth lattices plays the determining role in influencing the conductivity properties.[22] In the present case, it is clear that the carbon atoms with short intermolecular contacts possess *π*-orbitals which are oriented for efficient overlap in radicals **12** and **13**. The previously reported (well-spaced) compounds (**1**−**6**, **9**−**11**) are structurally different from each other, but none of them exhibits a continuous array of *π*-stacked neighboring phenalenyl units with intermolecular carbon···carbon contacts shorter than the van der Waals distances for the carbon atoms (3.4 Å). Examination of the packing of molecule **12** reveals that phenalenyl units of nearest neighbor molecules are parallel to each other and are involved in a superimposed *π*-overlap by selective registry between all six pairs of spin-bearing carbon atoms. Thus there is almost complete superposition of all six active carbon atoms of the phenalenyl nucleus with all intermolecular distances between the spin-bearing carbon centers well below the sum of the van der Waals atomic separations for carbon (Figure 3b), with closest C···C distance of 3.18 Å at 100 K. This configuration minimizes the steric interference and maximizes the overlap between the singly occupied molecular orbitals (SOMOs) of the adjacent phenalenyl units. By repeating this superimposed *π*-overlap, molecule **12** forms a highly symmetrical *π*-chain structure along [2 0 1], and this spiro-conjugated pathway corresponds to the long axis of the crystal (Figure 3a).

Thus the solid-state packing of **12** is very similar to that observed for radical **8**, which forms a highly symmetrical *π*-chain-type structure by repeating the superimposed *π*-overlap along the [1 0 1] direction but at slightly greater intermolecular C···C distances (3.28−3.36 Å).[27] In **12**, the mean plane separation between the superimposed *π*-overlapping phenalenyl units is 3.17 Å (100 K, Figure 3b), and this increases to 3.22 Å at higher temperature (293 K) and may be compared with values of 3.27 Å (100 K) and 3.32 Å (300 K) found in **8**.

The ethyl radical (**1**) exists as an isolated *π*-dimer with a mean plane separation of 3.18 Å in its spin-paired diamagnetic state at 100 K, while the paramagnetic state shows a mean plane separation of 3.35 Å at 293 K; thus the mean plane separations in **12** are shorter than those in **1**, and this point is discussed further below.

In the crystal lattice of molecule **12**, there is another weak interaction along the [0 1 0] direction. The molecules form a *π*-step stack along the *y*-axis (see Figure S1 in Supporting Information), and the packing of **12** in the *y*-direction can be compared to that observed for the benzyl radical (**7**) which packs in a 1-D *π*-step structure along the *y*-axis.[24] Nevertheless, for **12**, the closest intermolecular carbon···carbon distance (3.38 Å, Figure 5) along the *y*-direction between slipped pairs of spin-bearing carbon atoms is shorter than in the case of **7** (3.47 Å) but is exactly the same as that observed in the case of **8** at 223 K along the *y*-direction.[27]

The two phenalenyl units in radical **12** are involved in equivalent *π*-overlap with adjacent phenalenyl units of nearest neighbors. However, in the case of radical **13**, the presence of the 5-methyl substituents sterically hinders this type of close-packed *π*-overlap; the result is a compromise in which one phenalenyl unit aligns to give a superimposed *π*-overlap between the neighboring phenalenyl unit (as in **12**) but with a bend at the oxygen atoms, whereas the other phenalenyl adopts a slipped *π*-overlap structure, as shown in Figure 6. In the superimposed *π*-overlap interaction in **13**, all of the six spin-bearing carbon atoms of the adjacent phenalenyl units are in registry (Figure 6a), whereas in the slipped *π*-structure, only two pairs of fully spin-bearing carbon atoms of adjacent phenalenyl units are in registry (Figure 6b). Even in the bent, fully superimposed structure, the methyl groups severely compromise the approach of the two phenalenyl units involved in the *π*-overlap, and it is apparent from Figure 6b that the phenalenyl units are slightly bowed so that the central carbon atoms (C13 and C17, Figure 2b) approach much more closely (3.14 Å, Figure 6a) than the carbon pairs at the ends of the molecules; this leads to a mean plane separation for the superimposed *π*-structure of 3.26 Å.

In the case of the slipped, partial *π*-overlap between phenalenyl units in **13**, there is registry between each of the central carbons and three of the fully spin-bearing carbon atoms. In fact, the zero value of the spin density found at the central carbon in the simple HMO calculation is accidental; this is an active position, and more sophisticated calculations indicate a finite spin density at the central carbon atom of phenalenyl. For example, an early valence bond calculation on the parent phenalenyl radical found spin densities of $\rho_1 = 0.32$, $\rho_2 = -0.18$, $\rho_{3a} = -0.22$, and $\rho_{9b} = 0.26$;[44] note that it is only the carbon atoms with positive spin density that are in registry (Figure 4b).

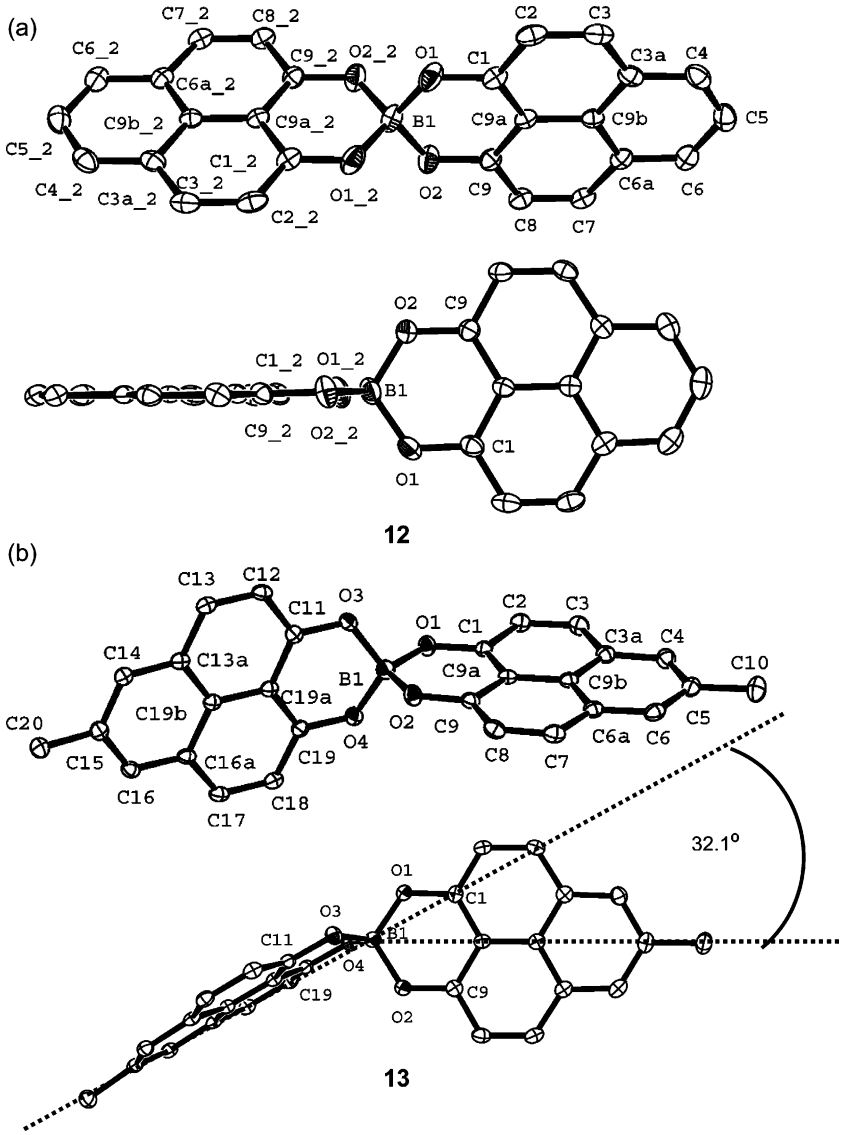

Figure 2. ORTEP diagrams and normalized view of radicals (a) **12** and (b) **13**. One of the phenalenyl units in **13** undergoes severe bending (32.1°) at two of the oxygen atoms (O3 and O4), unlike **12**, in which the phenalenyl units remain essentially planar.

The alternating scheme of π-overlaps in **13** is attributed to the presence of the methyl substituent, which leads in one case to a bend of the molecules so as to minimize the steric interaction of the methyl group with the oxygen of the other molecule involved in the π-dimer. The slipped structure arises for a similar reason—the methyl group cannot be avoided by a second bend in the molecule, and so the molecules of the π-dimer translate to reduce this steric interaction.

In **13**, the closest C···C distances between phenalenyl units at 100 K are 3.14 Å for superimposed π-overlap and 3.28 Å for partial π-overlap, respectively. At low temperature (100 K), the mean plane separations are 3.26 and 3.29 Å, whereas this parameter increases to 3.30 Å at 300 K for the superimposed and partial π-overlap interactions. These separations may be compared with the mean plane separation (3.35 Å) observed in the ethyl radical (**1**) in its high-temperature paramagnetic state at 293 K.[21] The distances between the phenalenyl rings (Figure 6) in both modes of overlap are within the van der Waals distance for carbon atoms (3.4 Å). The molecules of **13** form a π-chain as observed for molecule **12** but by alternating superimposed and partial π-overlap along [4, −1, −1] (Figure 4), which corresponds to the needle axis of the crystal.

In the crystal lattice of **13**, there is another weak interaction along the direction of the *x*-axis. Those phenalenyl units that take part in the superimposed π-overlap also stack in the direction of the *x*-axis, as shown in Figure 7, leading to a closest distance of 3.41 Å which occurs between two pairs of spin-bearing carbon atoms of two parallel phenalenyl units. Those phenalenyl units that take part in the partial π-overlap exhibit poor interchain interactions with a closest distance of 3.61 Å. Thus in the crystal lattice of **12** and **13**, the molecules form quasi two-dimensional structures which are dominated by 1-D π-chains with very short intermolecular contacts, providing an obvious pathway for conduction. Particularly in the case of **12**, the structures of these compounds are strongly related to that of **8**, in which the superimposed 1-D π-chains also dominate the packing.

(44) McConnell, H. M.; Dearman, H. H. *J. Chem. Phys.* **1958**, *28*, 51−53.

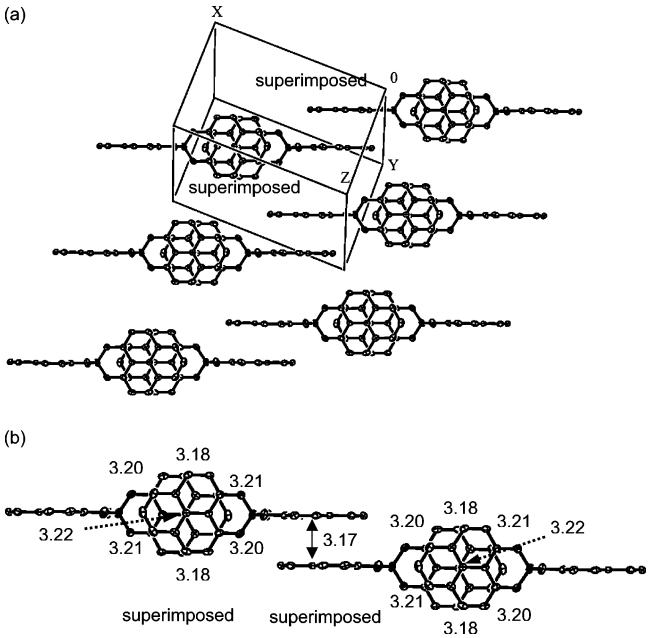

Figure 3. (a) Extended representation of solid-state packing of **12** showing that a single type of repeating superimposed π-overlap leads to an infinite spiro-conjugated chain in the crystal lattice, and (b) the closer view of the π-chain of **12**; the selective, symmetrical, and continuous π-overlap between all six pairs of spin-bearing carbon atoms of the adjacent phenalenyl units form a polymeric π-chain in the solid state with an interplanar separation between the adjacent phenalenyl units of 3.17 Å at 100 K.

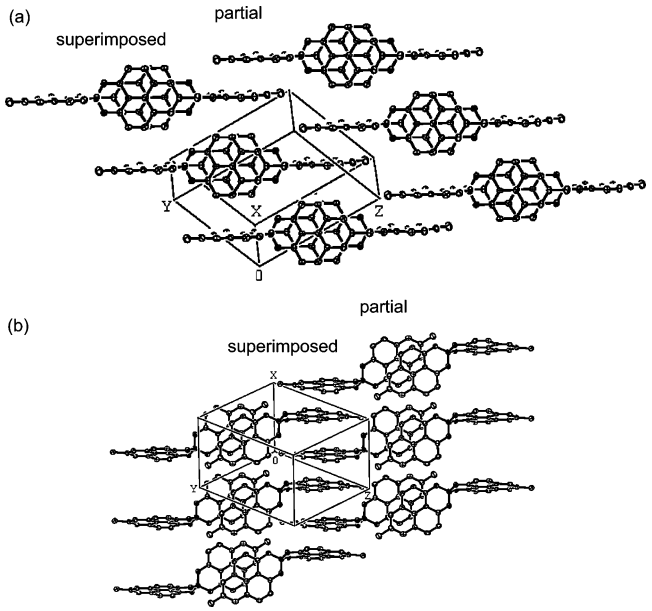

Figure 4. Extended representation of solid-state packing of **13** showing (a) superimposed π-overlap, and (b) partial π-overlap. These two types of alternating π-overlap lead to an infinite spiro-conjugated chain in the crystal lattice.

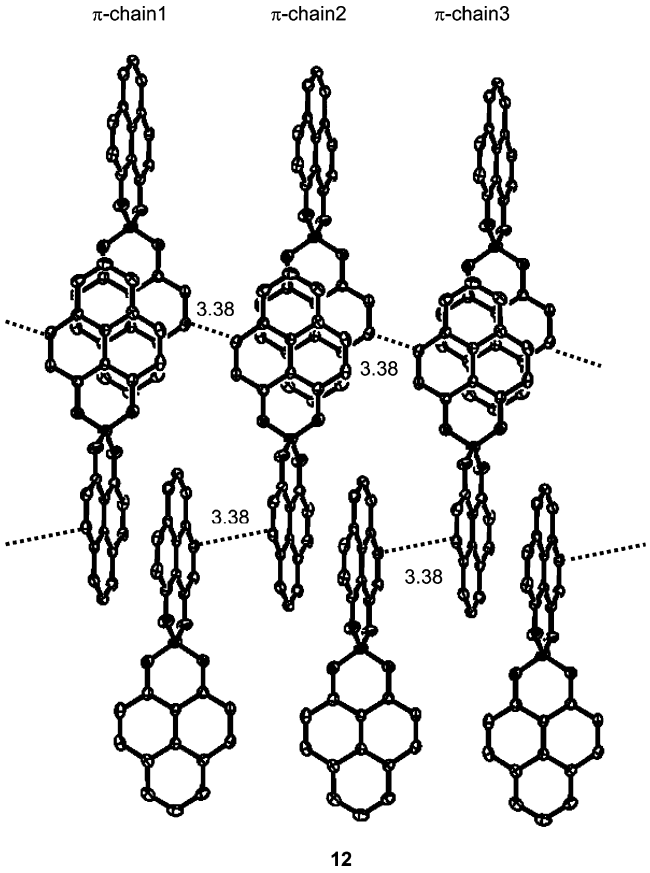

Figure 5. The stacked π-chains interact through a pair of spin-bearing carbons in each phenalenyl unit along the *y*-direction in the crystal lattice of **12** with a separation of 3.38 Å at 100 K.

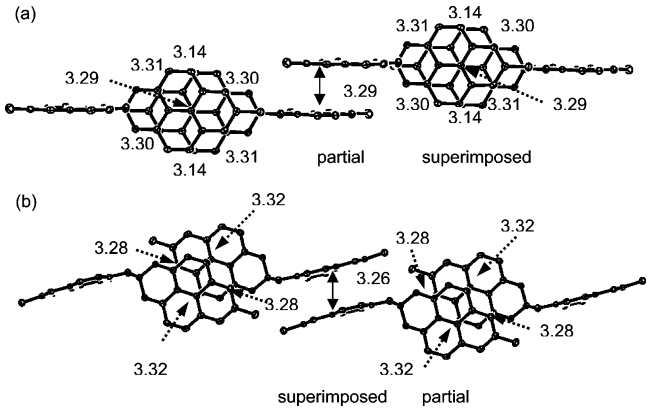

Figure 6. The continuous π-chain observed in the crystal lattice of **13** forms an alternate superimposed and partial π-overlap: (a) superimposed π-overlap showing that all six pairs of spin-bearing carbon atoms of the adjacent phenalenyl units interact with each other with a closest distance of 3.14 Å, and (b) partial π-overlap showing that only two pairs of spin-bearing carbon atoms of the adjacent phenalenyl units interact with each other at a distance of 3.28 Å at 100 K.

Magnetic Susceptibilities of 12 and 13. The temperature dependence of the magnetic susceptibilities (χ) of **12** and **13** was measured over the range of 8−330 K and is shown in Figure 8a and 8b as the paramagnetic susceptibility (χ_p, after correction for the sample diamagnetism). In compound **12**, χ_p increases with decreasing temperature below 330 K and reaches a broad maximum at $T_{max} = 150$ K. Because of the uniform chain-like structure of **12**, we used the Bonner−Fisher model for the $S = 1/2$ antiferromagnetic Heisenberg chain of isotropically interacting spins[45] in analytical representation to fit $\chi(T)$ [46] in the temperature range of 50−330 K (Figure 8a and 8b), and we obtained an intrachain exchange constant, $J = -86$ cm^{-1}, for compound **12**, a sign of strong antiferromagnetic interaction.

(45) Bonner, J. C.; Fisher, M. E. *Phys. Rev.* **1964**, *135*, A640−A658.

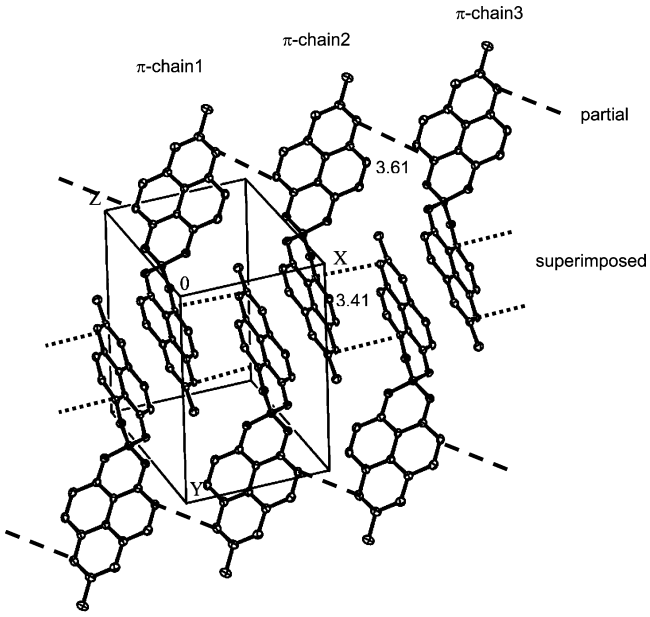

Figure 7. In **13**, the phenalenyls with superimposed π-overlap also interact along the direction of the *x*-axis with closest contacts of 3.41 Å between π-chains at 100 K.

For compound **13**, χ_p increases with decreasing temperature between 330 and 40 K, but at a rate more slowly than would be expected for a Curie paramagnet; for $T < 25$ K, there is a sharp growth in χ due to paramagnetic impurities (defects). To fit the data for compound **13**, we utilized the $S = 1/2$ alternating antiferromagnetic Heisenberg chain model,[47] in which the antiferromagnetic interaction along the chain alternates between values of J and αJ ($0 \leq \alpha \leq 1$); a Curie-type impurity term was introduced to account for the low-temperature paramagnetic tail.[24] The best fit to the data for compound **13** in the temperature range of 20−330 K was obtained with parameters $J = -59$ cm^{-1}, $\alpha = 0.8$, and a concentration of 2.94% of paramagnetic impurity sites per formula unit. The impurity term dominates the magnetic susceptibility at low temperatures, masking the antiferromagnetic character of the host molecules, although the antiferromagnetic character is evident from Figure 8c, which shows the effective fraction of Curie spins per molecule ($\chi_p T$/0.375) as a function of temperature. At high temperatures, these values approach the Curie free-spin value of one unpaired electron per molecule, a signature of the neutral radicals we have reported previously.[20,21,24−26] With decreasing temperature, $\chi_p T$/0.375 deviates strongly from the Curie model due to the very strong antiferromagnetic spin−spin interaction, which arises from the continuous array of overlapping π-stacked neighboring phenalenyl units in the structures of **12** and **13**.

Thus it is clear that the magnetism of these compounds is dominated by the 1-D antiferromagnetic coupling along the π-chains. In the case of **12**, the uniform Heisenberg model is appropriate as the radicals spin couple through a single type of interaction (fully superimposed π-overlap, Figure 3), while the alternating antiferromagnetic Heisenberg model is applicable to compound **13** because of the alternating mode of spin coupling (superimposed and partial π-overlap, Figures 4 and 6). The antiferromagnetic coupling along the 1-D chains dominates the magnetic susceptibility at low temperatures, although contributions from alternative magnetic pathways involving interchain coupling cannot be completely excluded as it can be seen that the 1-D chains in **12** and **13** interact with neighboring chains through two pairs of spin-bearing carbon centers. The 1-D chains of **12** interact with each other through two pairs of spin-bearing carbon centers on the two different phenalenyl units of the molecule (Figure 5) at a distance of 3.38 Å, while the interchain interaction of **13** arises from the interaction of two pairs of spin-bearing carbon centers on the phenalenyl unit, which is involved in the superimposed interaction (distance of 3.41 Å, see Figure 7)—these distances are close to the sum of the van der Waals atomic separations for carbon (3.4 Å).

Electrical Resistivity of 12 and 13. The single-crystal electrical conductivities (σ) of **12** and **13** were measured using a four-probe configuration, and the temperature dependence of the conductivity is shown in Figure 8d. A number of crystals were evaluated with similar results. The values of the room temperature conductivities are $\sigma_{RT} = 0.1$ S/cm (**12**) and $\sigma_{RT} = 0.3$ S/cm (**13**). These values, together with that of **8** ($\sigma_{RT} = 0.3$ S/cm),[27] are among the highest obtained for any neutral organic solid and are about 1 order of magnitude higher than previously reported neutral radical conductors **1** ($\sigma_{RT} = 1.0 \times 10^{-2}$ S/cm), **3** (2.4×10^{-2} S/cm), **5** (4.9×10^{-2} S/cm), **9** (4×10^{-2} S/cm), and **10** (1×10^{-2} S/cm),[20,21,26] and significantly higher than **2** (1.4×10^{-6} S/cm) and **4** (4×10^{-7} S/cm).[22,23] The conductivity data show semiconducting temperature dependence with activation energies of $\Delta = 0.24$ eV for **12** and 0.12 eV for **13**.

Optical Measurements of 12 and 13. To obtain further information on the electronic structure, we measured the transmission spectra of single crystals of **12** and **13** (Figure 8e). The most important feature in the transmission spectra is a strong increase of absorption below 0.38 eV (E_g) for radical **12** and 0.37 eV (E_g) for radical **13**. For compound **12**, the transmission reaches a plateau at 0.25 eV (E_g'), while in the case of compound **13**, the absorption extends deep into the phonon part of the spectrum (below 0.1 eV), making the exact determination of the band edge (E_g') impossible in our experiments. In the case of an intrinsic semiconductor, the measured optical band gap (E_g or E_g') can be correlated with the activation energy (Δ) calculated from the temperature dependence of the conductivity according to $E_g \approx 2 \times \Delta$.

Band Electronic Structures of 12 and 13. To address the question of solid-state packing and the conductivity measured for **12** and **13**, we carried out extended Hückel theory (EHT) band structure calculations[48] on the crystal structures. Such calculations have been very useful in understanding the electronic structure of the organic molecular superconductors[30,49] and thin-film field effect transistors,[31] but it should be noted at the outset that there are certain objections to the application of tight binding band theory to the neutral radical molecular conductors,[20] in that the calculations are unable to correctly describe the open shell electronic structure of some of these compounds.

A characteristic feature of the previously reported radicals has been the very narrow bandwidths found with the EHT

(46) Estes, W. E.; Gavel, D. P.; Hatfield, W. E.; Hodgson, D. J. *Inorg. Chem.* **1978**, *17*, 1415−1421.
(47) Duffy, W.; Barr, K. P. *Phys. Rev.* **1968**, *165*, 647−654.
(48) Hofmann, R. *Solids and Surfaces*; VCH: New York, 1988.
(49) Williams, J. M.; Ferraro, J. R.; Thorn, R. J.; Carlson, K. D.; Geiser, U.; Wang, H. H.; Kini, A. M.; Whangbo, M.-H. *Organic Superconductors (Including Fullerenes)*; Prentice Hall: Englewood Cliffs, NJ, 1992.

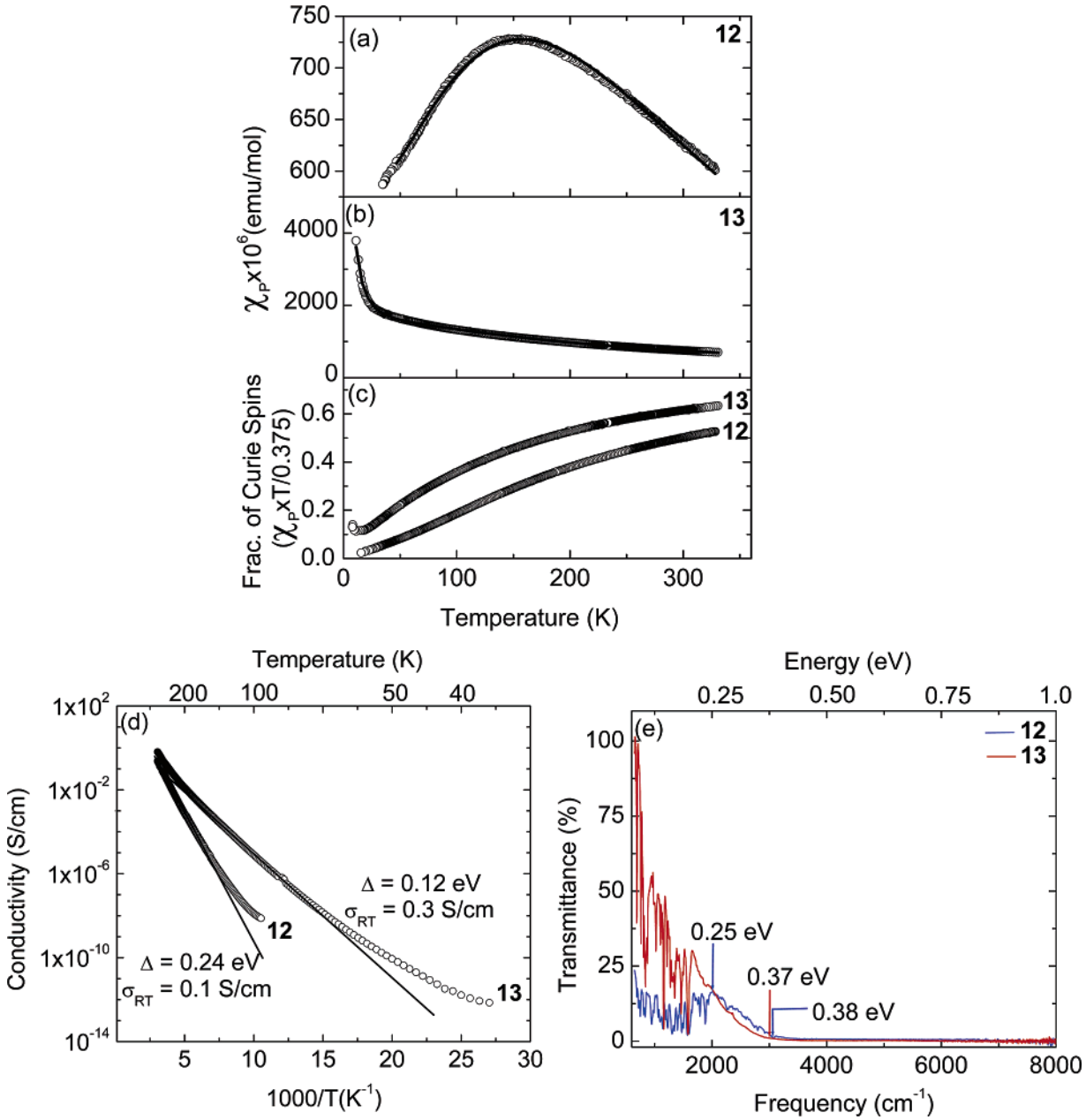

Figure 8. Solid-state properties of crystalline **12** and **13**. Paramagnetic susceptibility as a function of temperature, where the solid lines represent fits to the $S = {}^1/_2$ Heisenberg chain model: (a) uniform exchange coupling, **12**, (b) alternating exchange coupling, **13**. (c) Fraction of Curie spins as a function of temperature. (d) Single-crystal conductivity as a function of temperature. (e) Single-crystal near- and mid-infrared transmission spectra.

calculations. The band dispersions found for these compounds are always less than 0.1 eV, whereas most organic metals show EHT bandwidths in the range of 0.5−1.0 eV.[30,31,49] Although **1** and **3** exist as π-dimers, this mode of packing does not extend through the crystal lattice, and these molecules sit in the lattice as isolated dimers, in much the same fashion that **2**, **4**, **5**, and **9**−**11** pack as isolated monomers. However, the packing in the solid state of **7** and particularly **8**, **12**, and **13** is entirely different with a well-developed and continuous π-overlap extending along one of the directions in the crystal, sometimes in conjunction with strong secondary interactions in other directions. Where the long axes of the molecules are aligned in a parallel orientation, we show that the nodal character of the SOMO leads to three well-defined modes of π-overlap, all three of which are exemplified in the structures of **7**, **8**, **12**, and **13**.

Radical **7** crystallizes in a 1-D π-step structure with substantial band dispersion (0.37 eV, along b*) and displays Heisenberg antiferromagnetism; given the absence of a superlattice, the structure is indicative of metallic character.[24] However, radical **7** exhibits semiconducting behavior with a room temperature conductivity of $\sigma_{RT} = 1.4 \times 10^{-3}$ S/cm, which is very difficult to reconcile with the structure and remaining physical properties. Radical **8** crystallizes as a highly symmetric spiro-conjugated π-chain along the [1 0 1] direction, and within the chain, the C···C distances between repeating π-dimers are in the range of 3.28−3.36 Å, and **8** displays the temperature-independent Pauli paramagnetism characteristic of a metal.[27] The EHT band structure and density of state (DOS) calculations on the crystal lattice of **8** indicated a finite DOS at the Fermi level (metallic character) with substantial band dispersions along the three

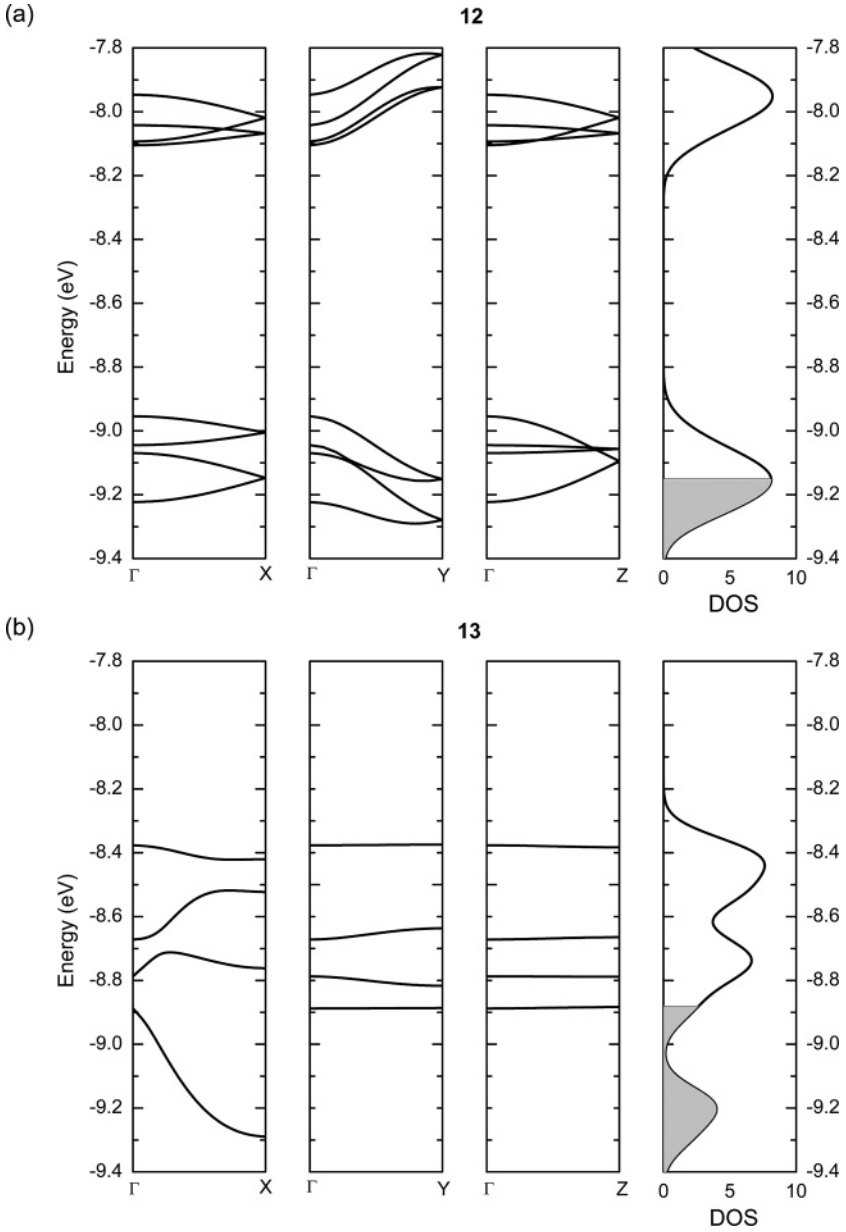

Figure 9. Calculated band structures of (a) crystalline **12** and (b) crystalline **13** based on X-ray structures determined at 100 K.

principal directions in reciprocal states with a bandwidth of ~0.5 eV. Nevertheless, radical **8** shows semiconducting behavior with an activation energy of 0.054 eV. We suggested that this apparently contradictory behavior can be resolved in terms of the resonating valence bond (RVB) ground state originally suggested by Pauling, but with the modifications introduced by Anderson.[32,33] The most characteristic feature of the RVB ground state is the presence of a high symmetry structure stabilization by resonance over a number of different structures. The spin coupling involved in the resonance structures might be quite complex in compounds such as **8**, where a number of different inter-carbon electron-pair bonds are possible, allowing resonance among many pairs of intermolecular (carbon−carbon) bonds.

Figure 9 shows the band structures and DOS calculated for the lattices found in the X-ray crystal structures of **12** and **13** at 100 K. The bands (eight bands for **12** and four bands for **13**) are derived from the two LUMOs of $\mathbf{12}^+$ or $\mathbf{13}^+$ for each of the molecules in the unit cell (four molecules for **12** and two molecules for **13**); these basically consist of spiro-conjugated symmetric and antisymmetric combinations of the 1,9-disubstituted phenalenyl LUMO.[20,39] Alternatively, they can be viewed as arising from the nonbonding molecular orbitals[6,7] of each of the phenalenyl units in the unit cell (eight phenalenyl units for **12** and four phenalenyl units for **13**). In a band picture, these orbitals (eight for **12** and four for **13**) now accommodate a total of four electrons for **12** and two electrons for **13**, leading to a quarter-filled band complex and a finite DOS at the Fermi level (metallic character).

It may be seen that the band dispersions found for **13** are higher than those in **12**; the maximum dispersions are 0.08 eV (along a*), 0.21 eV (b*), and 0.14 eV (c*) in **12** and 0.36 eV (along a*), 0.03 eV (b*), and 0.001 eV (c*) in **13**; note that **7**, **8**, **12**, and **13** show a quasi 1-D electronic band structure, and the absence of charge- or spin-density wave distortions is surprising. Typically, the conductivity in molecular conductors

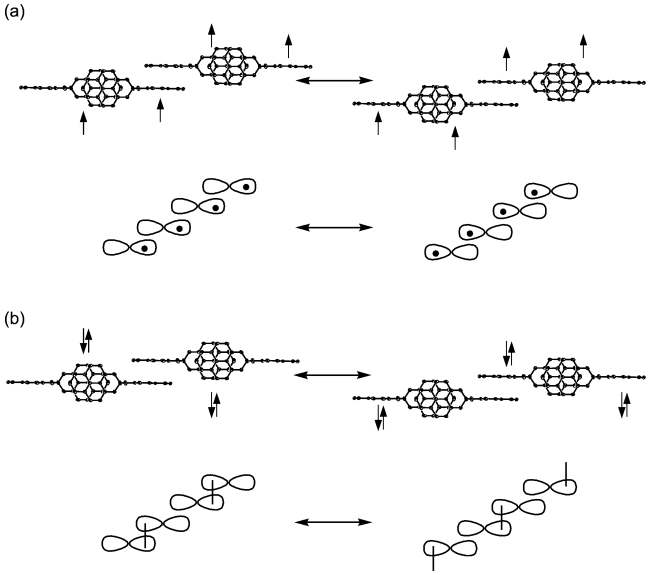

Figure 10. (a) Lewis free radical resonance structures for **12** and **13** and (b) the corresponding RVB resonance structure for **12** and **13**. The spiro-biphenalenyl structure is simplified to a figure eight for convenience.

depends on the relationship between the bandwidth (W) and the on-site Coulomb correlation energy (U), which often determines the activation energy for the conductivity (Δ), so that $\Delta \approx U$; U is primarily a molecular property that is often related to the disproportionation potential ΔE^{2-1} and is similar for radicals **12** and **13** (Table 1), whereas the transport energy gaps are found to be $\Delta = 0.24$ eV (**12**) and 0.12 eV (**13**). The bare value of U provides a lower bound for Δ, and the bandwidths (W), which are subject to solid-state packing effects, play the determining role in the relative conductivity values. The large transfer integrals implied by the bandwidth ($W \sim 1.2$ eV) observed for radical **13** as compared to the bandwidth ($W \sim 0.53$ eV) observed for radical **12** explain the improved conductivity for **13**.

The bandwidth W for **13** originates from strong atomic (or molecular) orbital interactions that lead to broad electronic energy bands in the solid state. Radical **13** is the first among the phenalenyl-based neutral radical conductors to possess a large bandwidth in the solid state (greater than 1 eV).

On the basis of the structural data, we give a representation of the spiro-conjugated one-dimensional π-chains in **12** and **13**, which shows the resonance of the unpaired electron between each phenalenyl unit in the molecules (Figure 10a).[39] However, the short C···C intermolecular distances support the idea of coupling the spins into electron pair bonds (Figure 10b). On the basis of the magnetic susceptibility data for **12** and **13**, it is clear that there is strong antiferromagnetic coupling along the π-chains of both compounds, but we find no evidence for the type of two-electron localization scheme shown in Figure 10b; instead these seem to be equally contributing resonance structures.[27]

In solution, the delocalization of the unpaired electron between the spiro-conjugated phenalenyl units in these radicals has been established by ESR studies.[39] Radical **12** is found to be paramagnetic, but with the spin density distributed over the whole molecule, so that on the time scale of the experiment the electron interacts with all of the nuclei in the molecule.[20,39] Similar results have been obtained from the solution ESR spectroscopy of radical **13** (see Figure S2 in Supporting Information), which demonstrates extensive hyperfine coupling, indicating a complete delocalization of spin over the whole molecule. These observations suggest that the two phenalenyl units do not act independently but are quite strongly coupled insofar as the lowest unoccupied molecular orbital (LUMO) is concerned.[28]

In the solid state, we used the structural data in order to check localization of the unpaired electron. In **12**, the two phenalenyl units of the molecule are equivalent by symmetry; in the case of **13**, the symmetry is broken in two ways: one phenalenyl is planar while the other is bent at the oxygen atoms, and the nature of the overlap is distinct with one fully superimposed π-overlap and one partial π-overlap, although the mean plane separations are remarkably similar, 3.26 and 3.29 Å (100 K) and 3.30 and 3.30 Å (300 K). To check for localization of the spins, we calculated the standard deviations of the bond length differences between the two halves of the phenalenyl unit on either side of the spiro-linkage in molecule **13**, reasoning that localization of the spin or charge would lead to larger standard deviation between formally equivalent bonds than would be observed in the case where complete delocalization of spin occurs.[50] It was observed previously that the standard deviation of the bond length differences between the two halves of the dimeric radicals **1** and **3** provides an indicator for the location of the charge and spin, and this established that the electron is preferentially localized in a particular half of the molecule resulting in bistability in these systems due to the existence of diamagnetic and paramagnetic dimers.[21,50] A similar calculation of the standard deviation of the bond length differences in **13** suggests that in the solid-sate the electron is delocalized in a SOMO extending over the whole molecule, as also observed by solution ESR spectroscopy. Thus the electronic structure of **12** and **13** is fully delocalized, in good agreement with the expectations of the resonating valence bond model.[27,32,33,51]

Conclusion

A new family of spiro-bis(1,9-disubstituted phenalenyl)boron neutral radical conductors based on the O,O-ligand system has been synthesized, characterized, and the solid-state properties have been investigated. In the solid state, these radicals neither remain strictly monomeric nor do they form isolated σ- or π-dimers, and the structures show that these radicals pack in a continuous array of π-stacked neighboring phenalenyl units with very short intermolecular carbon···carbon contacts, thus providing an obvious pathway for conduction. Magnetic susceptibility measurements support the idea that the radicals do not exist as isolated free radicals, and there is significant spin−spin interaction between the molecules in the solid state, as expected from the crystal structures. The disproportionation energies, which largely determine the on-site Coulombic correlation energy in the solid state in this class of radicals, are significantly lower than those of the spiro-bis(1,9-disubstituted phenalenyl)boron neutral radicals based on the N,O-ligand or N,N-ligand systems reported previously. This is reflected in the measured conductivities of this new class of materials, which are among the highest of any neutral organic solid. These are the first of the

(50) Chi, X.; Tham, F. S.; Cordes, A. W.; Itkis, M. E.; Haddon, R. C. *Synth. Met.* **2003**, *133*−*134*, 367−372.
(51) Fazekas, P.; Anderson, P. W. *Philos. Mag.* **1974**, *30*, 423−440.

wide band phenalenyl-based neutral radical conductors with bandwidths reaching greater than 1 eV, although the conductivity is still activated and this is best rationalized in terms of the resonating valence bond model. Thus it is clear that the conductivity of these neutral radicals can be strongly influenced by the solid-state packing, and there is considerable scope for improving the properties of these compounds.

Experimental Section

Materials. All reactions and manipulations were carried out under an atmosphere of dry argon using standard Schlenk and vacuum-line techniques; 1.0 M boron trichloride solution in CH_2Cl_2 (Aldrich) and sodium tetrakis[3,5-bis(trifluoromethyl)phenyl]borate (NaTFPB) (Boulder Scientific Company) were used as received. Tetrakis(dimethylamino)ethylene (TDAE) was purchased from Aldrich and distilled under argon prior to use. 9-Hydroxyphenalenone and 5-methyl-9-hydroxyphenalenone were synthesized according to literature procedures.[52] Dichloromethane was distilled from CaH_2 immediately before use. The NMR spectra were recorded on a Varian Inova 300 spectrometer. Chemical shifts downfield from the reference standard were assigned positive values. Cyclic voltammetric measurement was performed on a Pine AFCBP1 potentiostat using a Pt wire electrode in dry acetonitrile under argon atmosphere with *n*-Bu_4NPF_6 as the supporting electrolyte with a saturated calomel reference electrode. The ferrocenium/ferrocene couple was used as internal reference.

Preparation of 12^+Cl^-. 12^+Cl^- was prepared according to a modified literature procedure.[39] 9-Hydroxyphenalenone (0.98 g, 0.005 mol) in 1,2-dichloroethane (50 mL) was treated with boron trichloride (2.4 mL, 1 M solution in CH_2Cl_2, 0.0024 mol) under argon in the dark, and the mixture was stirred at 25 °C for 10 h. The bright yellow precipitate was separated by filtration, washed with cold dichloromethane (3 × 10 mL), and dried under reduced pressure to yield 1.03 g (98%) of the title compound. MS (MALDI) $m/z = 401$. IR (600−4000 cm^{-1}): 3069(w), 1622(s), 1601(s), 1572(s), 1541(w), 1501(m), 1476(m), 1442(w), 1423(m), 1362(w), 1347(m), 1311(vs), 1242(m), 1190(w), 1150(w), 1129(w), 1088(w), 1073(w), 1036(s), 961(m), 897(s), 856(s), 828(w), 769(w), 749(w), 721(w), 703(m).

Preparation of 13^+Cl^-. 5-Methyl-9-hydroxyphenalenone (1.05 g, 0.005 mol) in 1,2-dichloroethane (50 mL) was treated with boron trichloride (2.3 mL, 1 M solution in CH_2Cl_2, 0.0023 mol) under argon in the dark, and the reaction mixture was stirred overnight at room temperature under argon. The yellow solid was isolated by filtration (0.95 g, 89%). MS (MALDI) *m*/*z* 429. IR (600−4000 cm^{-1}): 3077(w), 3034(w), 2865(w), 1629(m), 1599(m), 1580(s), 1507(m), 1481(m), 1429(m), 1363(w), 1346(m), 1308(s), 1268(m), 1225(w), 1171(m), 1124(m), 1039(m), 965(m), 919(m), 887(s), 868(s), 836(m), 764(w), 722(w), 701(w).

Preparation of 12^+TFPB^-. A quantity of 0.45 g (5.1×10^{-4} mol) of solid sodium tetrakis[3,5-bis(trifluoromethyl)phenyl]borate (NaTFPB) was added to a solution of 12^+Cl^- (0.218 g, 5×10^{-4} mol) in 40 mL of dichloromethane. The mixture was stirred at 25 °C for 1 h, and a white precipitate formed during the reaction. The reaction mixture was filtered, and the filtrate was evaporated to dryness under reduced pressure. The crude product was purified by recrystallization from an ether/hexanes mixture, yielding 0.315 g (50%) of the analytically pure title compound. MS (MALDI) $m/z = 401$. ^1H NMR ($CDCl_3$): δ 8.66 (d, 4H), 8.48 (d, 4H), 7.96 (t, 2H), 7.70 (br s, 8H), 7.45 (s, 4H), 7.44 (d, 4H); signals also appear at δ 3.48 (q), 1.21 (t) due to the diethyl ether included in the lattice. IR (600−4000 cm^{-1}): 2984(w), 1625(m), 1600(m), 1574(s), 1503(w), 1477(m), 1457(w), 1422(w), 1353(s), 1311(s), 1275(vs), 1242(m), 1122(vs), 1088(w), 1071(w), 1055(w), 1030(s), 961(m), 896(m), 886(m), 852(s), 840(w), 766(w), 747(w), 715(m), 701(w), 683 (m). Anal. Calcd for $C_{58}H_{26}B_2O_4F_{24}\cdot 0.5C_4H_{10}O$: C, 55.36; H, 2.40. Found: C, 55.29; H, 2.27.

Preparation of 13^+TFPB^-. A quantity of 2.22 g (0.0025 mol) of solid sodium tetrakis[3,5-bis(trifluoromethyl)phenyl]borate (NaTFPB) was added to a dichloromethane (20 mL) solution of 13^+Cl^- (1.16 g, 0.0025 mol), and the resulting mixture was stirred for 2 h at 25 °C; a white precipitate formed during the reaction. The mixture was filtered and the solvent evaporated to give an orange solid. The solid was recrystallized as yellow plates from a 2:1 ether/hexane mixture (1.9 g, 59%). MS (MALDI) *m*/*z* 429. ^1H NMR (CD_3CN): δ 8.72 (d, 4H), 8.40 (s, 4H), 7.69 (br s, 8H), 7.66 (s, 4H), 7.51 (d, 4H), 2.70 (s, 6H). IR (600−4000 cm^{-1}): 3041(w), 2940(w), 2877(w), 1632(m), 1601(m), 1580(m), 1505(m), 1480(m), 1435(w), 1354(m), 1308(m), 1277(s), 1158(m), 1220(s), 1039(m), 963(m), 939(m), 910(m), 881(s), 839(m), 794(w), 767(w), 744(w), 714(m), 700(w). Anal. Calcd for $C_{60}H_{30}B_2O_4F_{24}$: C, 55.75; H, 2.34. Found: C, 56.09; H, 2.40.

Crystallization of 12. A solution of 64 mg of 12^+TFPB^- (5.1×10^{-5} mol) in 16 mL of dry acetonitrile was placed in a container (25 mL round-bottom flask), and 30 mg of TDAE (15.0×10^{-5} mol) was dissolved in 15 mL of dry acetonitrile in another container (25 mL round-bottom flask). The containers were attached to an invertible H-cell in a glovebox. The H-cell was removed from the glovebox and attached to a vacuum line, and the containers were taken through three cycles of freeze, pump, and thaw to degas the solutions. The H-cell was inverted slowly, and the solutions were allowed to diffuse through the glass frit. After sitting in the dark for 2 days, the cell yielded 7 mg of black shining crystals. IR (600−4000 cm^{-1}): 3051(w), 1629(m), 1587(s), 1547(s), 1497(m), 1438(s), 1396(m), 1356(m), 1324(w), 1306(m), 1262(s), 1242(w), 1218(s), 1188(w), 1138(m), 1113(m), 1067(w), 964(s), 849(w), 837(w), 750(w), 681(w). Anal. Calcd for $C_{26}H_{14}BO_4$: C, 77.83; H, 3.52. Found: C, 76.57; H, 3.35.

Crystallization of 13. A solution of 65 mg (5.0×10^{-5} mol) of 13^+TFPB^- in 17 mL of dry acetonitrile was placed in a container (25 mL round-bottom flask), and 25 mg (12.0×10^{-5} mol) of TDAE dissolved in 15 mL of dry acetonitrile was placed in another container (25 mL round-bottom flask). The containers were attached to an invertible H-cell in the glovebox. The H-cell was removed from the glovebox and attached to the vacuum line, and the containers were taken through three cycles of freeze, pump, and thaw to degas the solutions. The H-cell was inverted slowly, and the solutions were allowed to diffuse through the glass frit. After sitting in the dark for 3 days, the cell yielded 9 mg of black shining crystals. IR (600−4000 cm^{-1}): 3036(w), 2976(w), 2917(w), 1632(m), 1591(m), 1561(s), 1501(m), 1438(m), 1409(m), 1377(w), 1356(m), 1300(m), 1278(m), 1248(s), 1157(s), 1128(w), 1100(m), 1016(m), 960(m), 909(s), 853(s), 792(m), 751(w), 720(w), 688(m). Anal. Calcd for $C_{28}H_{18}BO_4$: C, 78.34; H, 4.23. Found: C, 77.77; H, 4.11.

X-ray Crystallography. Data were collected on an X8-APEX Bruker Kappa four circles X-ray diffractometer system (Mo radiation, $\lambda = 0.71073$ Å) for **12** at 100 and 293 K. The X-ray data for **13** were collected on a Bruker APEX2 (version 1.0−22) platform CCD X-ray diffractometer system (Mo radiation, $\lambda = 0.71073$ Å). The crystals were mounted onto a glass fiber with epoxy resin. The crystallographic parameters and unit cell dimensions are summarized in Table 2. Absorption corrections were applied to the raw intensity data using the SADABS program.[53] Atomic coordinates, isotropic and anisotropic displacement parameters of all the non-hydrogen atoms were refined by means of a full matrix least-squares procedure on F^2. The H-atoms were included in the refinement in calculated positions riding on the atoms to which they were attached. Full details, including bond lengths and bond angles, are given in the Supporting Information.

Magnetic Susceptibility Measurements. The magnetic susceptibilities were measured with a George Associates Faraday balance

(52) Haddon, R. C.; Rayford, R.; Hirani, A. M. *J. Org. Chem.* **1981**, *46*, 4587−4588.

(53) *SADABS*, 5.02 ed.; Bruker Analytical X-ray System, Inc: Madison, WI, 1997−1998.

operating at 0.5 T. The calculated diamagnetic susceptibilities (χ_0) are -223.7×10^{-6} emu/mol for **12** and -235.04×10^{-6} emu/mol for **13**.

Conductivity Measurements. The single-crystal conductivities of **12** and **13** were measured in a four-probe configuration. The in-line contacts were made with silver paint. The sample was placed on a sapphire substrate, and electrical connections between the silver paint contacts and substrate were made by thin, flexible 25 μm diameter silver wires to relieve mechanical stress during thermal cycling of the sample. The conductivities were measured along the long axis of the crystals, which were determined during the X-ray crystallographic studies. The temperature dependence of the conductivity was measured in the range of 92−327 K for **12** and 40−327 K for **13**. The data are presented for a crystal of **12** with dimensions of $2.7 \times 0.05 \times 0.02$ mm^3 and for a crystal of **13** with dimensions of $1.5 \times 0.8 \times 0.04$ mm^3. The same conductivity was observed with a thinner crystal of **12** with dimensions of $3.3 \times 0.05 \times 0.01$ mm^3 and crystal of **13** with dimensions of $1.5 \times 0.7 \times 0.05$ mm^3. The conductivity was measured in a custom-made helium variable-temperature probe using a Lake Shore 340 temperature controller. A Keithley 236 unit was used as a voltage source and current meter, and two 6517 Keithley electrometers were used to measure the voltage drop between the potential leads in a four-probe configuration; the instrumentation was driven with LabVIEW software.

Single-Crystal Near- and Mid-Infrared Transmission Spectroscopy. The infrared transmission measurements were carried out in a FTIR Nicolet Nexus 670 ESP spectrometer integrated with Continuum Thermo-Nicolet FTIR microscope.

Band-Structure Calculations. The band-structure calculations made use of a modified version of the extended Hückel theory (EHT) band-structure program supplied by M.-H. Whangbo. The parameter set is chosen to provide a reasonably consistent picture of bonding in heterocyclic organic compounds.[31,54]

Acknowledgment. This work was supported by the Office of Basic Energy Sciences, Department of Energy under Grant DE-FG02-04ER46138, and by DOD/DARPA/DMEA under Grant Number H94003-04-2-0404.

Supporting Information Available: Additional structural packing diagram, ESR spectrum of **13** in CH_2Cl_2 with numerical fit, complete set of fitting parameters to the magnetic susceptibility data of **12** and **13**, tables of crystallographic and structural refinement data, atomic coordinates, bond lengths, bond angles, and anisotropic thermal parameters (PDF). This material is available free of charge via the Internet at http://pubs.acs.org.

JA0560276

(54) Cordes, A. W.; Haddon, R. C.; Oakley, R. T.; Schneemeyer, L. F.; Waszczak, J. V.; Young, K. M.; Zimmerman, N. M. *J. Am. Chem. Soc.* **1991**, *113*, 582−588.